Path Integral over Equivalence Classes for Quantum Dynamics with Static Disorder

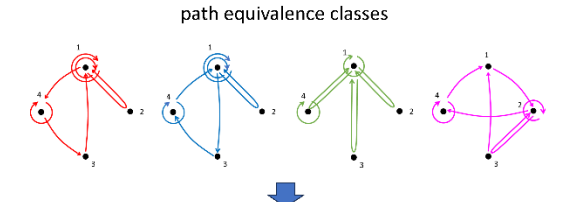
Nancy Makri*

Departments of Chemistry and Physics, University of Illinois 505 S. Mathews Avenue, Urbana, IL 61801

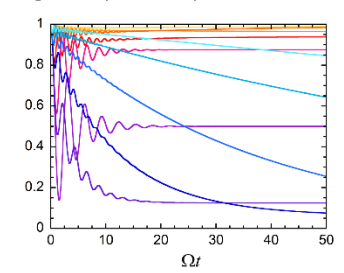
Abstract

An efficient, fully quantum mechanical real-time path integral method for including the effects of static disorder in the dynamics of systems coupled to common or local harmonic baths is presented. Rather than performing a large number of demanding calculations for different realizations of the system Hamiltonian, the influence of the bath is captured through a single evaluation of the path sum by grouping the system paths into equivalence classes of fixed system amplitudes. The method is illustrated with several analytical and numerical examples that show a variety of nontrivial effects arising from the interplay among coherence, dissipation, thermal fluctuations and geometric phases.

TOC image:



path integral for quantum dynamics with static disorder



The problem of simulating the dynamics of a small system interacting with a harmonic bath continues to attract much attention. Besides offering the simplest model that accounts for dissipative effects from condensed phase environments, 1-3 system-bath Hamiltonians can describe the progression of chemical processes along a reaction path, 4-5 the contributions of intramolecular vibrations and lattice phonons to tunneling dynamics, 6 vibronic effects in spectroscopy, charge and energy transfer in solution or biomolecules, 7 as well as many other phenomena of interest to chemistry, physics, biology and materials research. The ability of harmonic bath Hamiltonians to capture (qualitatively and often quantitatively) the effects of complex, anharmonic media on the dynamics of the observed system rests on the central limit theorem and forms the basis of the well-known Gaussian or linear response approximation, which is well-known in classical statistical mechanics 8 and has been derived for quantum mechanical environments 9 using path integral tools.

The path integral formulation of time-dependent quantum mechanics¹⁰⁻¹¹ is intuitive and particularly attractive for system-bath Hamiltonians because it allows any number of harmonic bath degrees of freedom to be integrated out analytically, at zero or any finite temperature, giving rise to a Gaussian influence functional¹² that modifies the amplitude of the system. However, the influence functional destroys the Markovian nature of the dynamics, introducing memory effects. Direct numerical evaluation of the real-time path integral requires computing astronomical numbers of terms, leading to exponentially increasing cost with the number of time steps, while Monte Carlo sampling techniques do not provide a viable alternative because the highly oscillatory nature of the quantum phase leads to a disastrous sign problem.¹³⁻¹⁴

Early work introduced the quasi-adiabatic propagator path integral (QuAPI), which uses a physically motivated partitioning of the propagator¹⁵ along with optimal grids¹⁶ based on discrete variable representations¹⁷ (DVR), and showed that the path integral expression for the reduced density matrix (RDM) of the system can be decomposed into a series of tensor multiplications, ¹⁸⁻¹⁹ achieving linear scaling with the total propagation time. The QuAPI tensors store the path integral variables over the memory length $L\Delta t$, where Δt is the path integral time step. For a system of n states (or DVR grid points), the iterative QuAPI algorithm formally requires the storage of n^{2L} elements. However, the damping effect of the influence functional causes the vast majority of paths to carry exponentially small weights in strongly dissipative regimes. Powerful filtering techniques have been developed for eliminating unnecessary storage of the QuAPI tensors.²⁰⁻²⁴ Further, the blip decomposition²⁵ offers a systematic way of selecting the contributing forward-backward path pairs, along with an exponential reduction of the number of terms within the memory interval. More recently, the time-evolving matrix product operator (TEMPO) algorithm²⁶ implemented singular value decomposition (SVD) techniques to compress the QuAPI tensors, obtaining matrix product representations of path amplitudes whose dimensions can be considerably smaller than n^{2L} in cases of underdamped dynamics. The quantumclassical path integral²⁷⁻²⁸ (OCPI), a rigorous formulation of quantum-classical dynamics that is applicable to processes in anharmonic environments, also offers a numerically exact, fully quantum mechanical algorithm for system-bath Hamiltonians, which is advantageous in situations with long memory.

Recent theoretical analysis²⁹⁻³⁰ showed that the QuAPI tensors can be further decomposed through a recursive shift of the entangled terms to longer time, until the entanglement of the path integral variables becomes vanishingly small (typically upon exceeding the memory length and sometimes even faster³¹). This decomposition replaces the QuAPI tensor multiplication by r_{max} multiplications of minimal-sized $n^2 \times n^2$ matrices, where r_{max} is the path integral entanglement length. The resulting small matrix path integral (SMatPI) algorithm is an exact, analytically derived decomposition that does not employ tensor compression. By eliminating the QuAPI tensor storage, SMatPI calculations converge easily in much larger systems and long-memory processes. The most demanding procedure is the

numerical evaluation of the SMatPI matrices, which involves path sums within the memory length that may be performed by any available method (for example, a full or filtered QuAPI sum, the blip sum, TEMPO, QCPI, or the kink sum³²). Propagation beyond the memory length is extremely efficient with the SMatPI algorithm and adds almost negligible cost, making SMatPI the method of choice for propagation of the RDM to long times.

The present Letter addresses the computational challenges encountered when accounting for the effects of static disorder on dynamical observables. In such situations one must perform a large number of similar calculations, each with different values of the system's site energies that are usually sampled from a Gaussian distribution. When the parameters are such that a single propagation of the RDM is expensive, obtaining such a statistical average may be computationally prohibitive.

It is shown that the cost of performing the path sum for each realization of the system's site energies can be alleviated by precomputing sums of influence functional components, which do not depend on the system Hamiltonian. Since path amplitudes are products of system propagator elements and influence functional factors, it appears that the former cannot be removed from the sum. However, by exploiting the structure of the path integral, it is shown that the components associated with the system Hamiltonian may be included *after* the influence functional terms have been summed. This is achieved by grouping the paths into equivalence classes based on the adjacency matrix (i.e. the connectivity) of each path. The method is ideally suited to the calculation of SMatPI matrices, in particular to the kink sum algorithm,³² which allows efficient evaluation of the path sum with very long memory.

In the conventional case where the system sites are coupled to a common bath, the system-bath Hamiltonian has the form

$$\hat{H}_{sb} = \hat{H} + \sum_{i} \frac{\hat{p}_{i}^{2}}{2m} + \frac{1}{2} m \omega_{i}^{2} \left(\hat{q}_{i} - \frac{c_{i} \hat{s}}{m \omega_{i}^{2}} \right)^{2}$$
 (1)

where

$$\hat{H} = \sum_{i=1}^{n} \sum_{j=1}^{n} H_{ij} \left| \varphi_i \right\rangle \left\langle \varphi_j \right| \tag{2}$$

is the Hamiltonian of the system, the discrete (or DVR-discretized) system operator is defined as

$$\hat{s} = \sum_{j=1}^{n} \kappa_{j} \left| \varphi_{j} \right\rangle \left\langle \varphi_{j} \right| \tag{3}$$

and q_i , p_i are the harmonic bath coordinates and momenta. A vector generalization of the system operator³³ allows local as well as correlated baths to be described by a system-bath Hamiltonian similar to Eq. (1). The elements of the $n^2 \times n^2$ RDM of the system for the initial condition $|s_0^-\rangle\langle s_0^+|$ are

$$\tilde{\rho}_{s_{\tau}^{+},s_{\alpha}^{+}}^{(N0)} \equiv \operatorname{Tr}_{\text{env}} \left\langle s_{N}^{-} \middle| e^{i\hat{H}t/\hbar} \middle| s_{0}^{-} \right\rangle \hat{\rho}_{\text{env}}(0) \left\langle s_{0}^{+} \middle| e^{-i\hat{H}t/\hbar} \middle| s_{N}^{+} \right\rangle. \tag{4}$$

In the discretized path integral formulation,³⁴ the RDM elements are given by multidimensional sums of amplitudes,

$$\tilde{\rho}_{s_{N}^{+}s_{0}^{+}}^{(N0)} = \sum_{s_{N}^{+}, =\sigma_{1}}^{\sigma_{n}} \cdots \sum_{s_{n}^{+}=\sigma_{1}}^{\sigma_{n}} K_{s_{N}^{+}, s_{N-1}^{+}} \cdots K_{s_{1}^{+}, s_{0}^{+}} K_{s_{N}^{-}, s_{N-1}^{-}} \cdots K_{s_{1}^{-}, s_{0}^{-}} F_{s_{N}^{+}, s_{N-1}^{+}, \dots, s_{0}^{+}}$$

$$(5)$$

along all discrete forward-backward paths $s_N^\pm \cdots s_0^\pm$ associated with the time points that separate short-time propagators. Here $K_{s_k^+s_{k-1}^+}$ are the forward-backward system propagator elments and $F_{s_k^\pm s_k^\pm}^{kk'}$ are the QuAPI-discretized influence functional factors.³⁵

In each term in Eq. (5), the total system component along the forward path, $K_{s_N^+, s_{N-1}^+} \cdots K_{s_1^+, s_0^+}$, depends only on the number of times each pair of connected sites appears in the path (see Figure 1). As a result, the set of paths can be divided into μ equivalence classes, each containing all the paths that in the absence of coupling to a bath have the same amplitude.

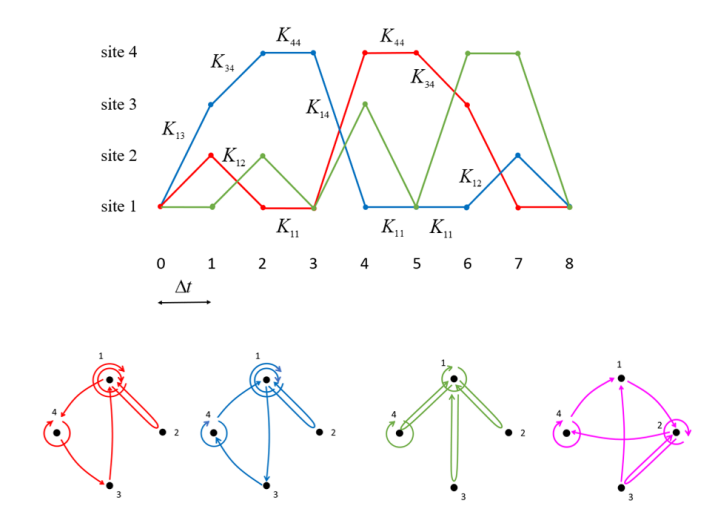


Fig. 1. Four paths with identical endpoints in a four-state system for N=8. The red and blue paths belong to the same equivalence class. In each of these paths the propagator elements K_{11} and K_{12} appear twice, while the elements K_{13} , K_{14} , K_{34} and K_{44} appear once. In the absence of the influence functional, these two paths have identical amplitudes. The green and magenta paths belong to different equivalence classes. Top: paths vs. time. (For clarity, the fourth path is not shown here.) Bottom: path graphs, where the vertices represent the system sites.

It follows that the influence functional factors can be summed within the memory interval separately from the system propagators if the terms are grouped into μ^2 forward-backward equivalence classes based on path connectivity. Once the sum over all paths has been performed for each equivalence class, the system propagators can be included according to the common system path amplitude of each class, producing the desired RDM from which SMatPI matrices are computed. Thus, the equivalence class formulation of the path integral (EqC-PI) expresses Eq. (5) for the RDM as a sum over the μ^2 equivalence classes that correspond to the forward and backward system paths,

$$\tilde{\rho}_{s_{N}^{\pm}s_{0}^{\pm}}^{(N0)} = \sum_{\alpha_{+}=1}^{\mu} \sum_{\alpha_{-}=1}^{\mu} S_{\alpha_{+}} S_{\alpha_{-}}^{*} G_{\alpha_{+}\alpha_{-}}$$

$$\tag{6}$$

where S_{α} is the amplitude of any system path in equivalence class lpha and

$$G_{\alpha_{+}\alpha_{-}} = \sum_{p_{\alpha_{+}}=1}^{m_{\alpha_{+}}} \sum_{p_{\alpha_{+}i}=1}^{m_{\alpha_{-}}} F_{p_{\alpha_{+}i}p_{\alpha_{-}j}}$$

$$(7)$$

is the total influence functional for the particular class, which is the sum of influence functionals over the $m_{\alpha_{+}}$ forward paths $p_{\alpha_{-}i} = \left\{s_{N}^{+}s_{N-1}^{+}...s_{0}^{+}\right\}_{\alpha_{-}i}$ and $m_{\alpha_{-}}$ backward paths $p_{\alpha_{-}j} = \left\{s_{N}^{-}s_{N-1}^{-}...s_{0}^{-}\right\}_{\alpha_{-}j}$. (Note that the dependence of these quantities on the value of N has been suppressed for clarity.)

As an analytical example, consider a symmetric two-level system (TLS) described by the Hamiltonian

$$\hat{H} = -\hbar\Omega(|\varphi_1\rangle\langle\varphi_2| + |\varphi_2\rangle\langle\varphi_1|) \tag{8}$$

which serves as the paradigm of coherent tunneling between the two sites φ_1 , φ_2 . Since the two site energies are identical in this case, there are only two independent propagator elements. For a path integral time step Δt , these are

$$K_{11} = K_{22} = \cos\Omega\Delta t, \quad K_{12} = i\sin\Omega\Delta t. \tag{9}$$

Table 1. Equivalence classes vs. the (even) number N of path integral steps for a symmetric TLS with identical, fixed endpoints. The columns show the composition of the path amplitude and the cardinality of each class, along with the total contribution to the diagonal element of the propagator $\langle \varphi | e^{-iH_0N\Delta t} | \varphi_1 \rangle$.

equivalence class α	number of K_{11} factors	number of K_{12} factors	path amplitude S_{α}	cardinality m_{α}	total contribution
$\alpha = 1$	N	0	K_{11}^N	$m_1 = 1$	K_{11}^N
$\alpha = 2$	N – 2	2	$K_{11}^{N-2}K_{12}^2$	$m_2 = \frac{N!}{2!(N-2)!}$	$m_2 K_{11}^{N-2} K_{12}^2$
$\alpha = 3$	N-4	4	$K_{11}^{N-4}K_{12}^4$	$m_3 = \frac{N!}{4!(N-4)!}$	$m_3 K_{11}^{N-4} K_{12}^4$
$\alpha = \frac{1}{2}N + 1$	0	N	K_{12}^N	$m_{\frac{1}{2}N+1} = 1$	K_{12}^N

Consider a path that starts and ends on state 1. For propagation to N time steps there are 2^{N-1} discrete paths. Because the endpoints are identical, state changes must come in pairs, and since the two diagonal propagator elements have equal values, the amplitude of a path is determined by the number of hops, dividing the set of paths into equivalence classes. It is straightforward to obtain the cardinality of each equivalence class by determining the number of paths that hop between the two sites once, twice, etc. Table 1 shows the equivalence classes with their cardinalities, as well as the composition and amplitude of paths in each class, for an even value of the path length N. In the absence of coupling to a bath, the influence functional along each path is equal to unity, thus $G_{\alpha,\alpha} = m_{\alpha} m_{\alpha}$ and therefore

$$\tilde{\rho}_{11,11}^{(N0)} = \sum_{\alpha=1}^{\mu} \sum_{\alpha=1}^{\mu} S_{\alpha_{+}} S_{\alpha_{-}}^{*} m_{\alpha_{+}} m_{\alpha_{-}} = \left| \sum_{\alpha=1}^{\mu} S_{\alpha} m_{\alpha} \right|^{2}$$
(10)

which is recognized as the squared modulus of the propagator at the time $N\Delta t$. It is easy to show that the total sum of amplitudes for the propagator equals $\cos(N\Omega\Delta t)$, which agrees with the exact value $\cos^2(N\Omega\Delta t)$ for the probability to remain on site φ_1 .

For an asymmetric TLS $(K_{11} \neq K_{22})$ the number of equivalence classes is $\frac{1}{2}(N-1)(N-2)+2$. The number of equivalence classes grows rapidly as the number of states increases. The classification of paths increases computer storage and may eventually become impractical, but for systems of a few states the approach described in this Letter offers a very efficient way of averaging dynamical results over a large number of Hamiltonian parameters.

Numerical evaluation of path sums can be performed by a number of methods, but generally the computational demands grow rapidly with the total number of time steps. Propagation to long times must be performed by iterative algorithms, which rely on the finite length of bath-induced memory. The most efficient iterative method is the SMatPI algorithm, which involves repeated multiplication of small, $n^2 \times n^2$ matrices. Even though the path integral variables in Eq. (5) are entangled within the memory length induced by the bath, the SMatPI decomposition²⁹⁻³⁰ disentangles them recursively, expressing the amplitude as a sum of small matrix products,

$$\tilde{\boldsymbol{\rho}}^{(N0)} = \sum_{r=1}^{N-1} \mathbf{M}^{(N,N-r)} \cdot \tilde{\boldsymbol{\rho}}^{(N-r,0)} + \mathbf{M}^{(N0)}$$
(11)

where $\mathbf{M}^{(N,N-r)}$ are the $n^2 \times n^2$ SMatPI matrices. Eq. (11) is, by construction, an exact decomposition of the path integral. The key idea in the SMatPI propagation algorithm is that the elements of these matrices decrease rapidly with the index (i.e. time) separation r and may be dropped beyond some entanglement length r_{max} , which in practice is equal to (but may also be smaller than) the memory length induced by the bath. Dropping the negligible residual leads to the following expression of the RDM at times longer than the entanglement length:

$$\tilde{\boldsymbol{\rho}}^{(N0)} = \sum_{r=1}^{r_{\text{max}}} \mathbf{M}^{(N,N-r)} \cdot \tilde{\boldsymbol{\rho}}^{(N-r,0)}, \quad N = r_{\text{max}} + 1, \dots$$
(12)

Typically, the SMatPI propagation algorithm is so fast that propagation to very long times occurs in negligible time in comparison with the costly generation of the SMatPI matrices from the values of the RDMs within the memory interval, as given by Eq. (5) for $N \le r_{\text{max}}$.

It is straightforward to group the system paths into equivalence classes in order to compute the RDMs required to construct SMatPI matrices. According to Equations (6) and (7), the summation with respect to system paths over the memory length (which is the most demanding part of a SMatPI calculation) does not include system components, and by adopting a suitable factorization of system-bath propagators that removes endpoint effects from the influence functional this sum needs to be performed and stored only once for each value of N. To obtain dynamical results that are statistically averaged with respect to static disorder, one samples disorder values according to the chosen (usually Gaussian) distribution, generating a series of system Hamiltonians. For each such Hamiltonian, RDMs are calculated by combining the precomputed influence functional sums after multiplying with the system amplitude pertaining to each equivalence class, as described in Eq. (6). SMatPI matrices are then generated from these RDMs according to the standard SMatPI procedure.

A few numerical examples help illustrate the algorithm, along with some nontrivial effects induced by static disorder on model systems. The states of the system Hamiltonian are coupled to a harmonic bath (or to separate baths) described by a spectral density of the common Ohmic form,

$$J(\omega) = \frac{1}{2}\pi\xi\omega e^{-\omega/\omega_{c}} \tag{13}$$

where ξ indicates the system-bath coupling strength and the maximum of Eq. (13) is at ω_c . The reorganization energy of a TLS coupled to a common bath, and also of each monomer in a molecular aggregate, is equal to $2\xi\hbar\omega_c$. Static disorder is included by averaging the RDMs computed for a large number of system Hamiltonians whose diagonal elements (the site energies) are given by the normal distribution with mean values equal to those of the target system and standard deviation σ ,

$$H_{ii} = \bar{H}_{ii} + \Delta \varepsilon_i, \quad P(\Delta \varepsilon_i) = \frac{1}{\sqrt{2\pi}\sigma^2} e^{-\frac{\Delta \varepsilon_i^2}{2\sigma^2}}.$$
 (14)

Static asymmetry can lead to highly asymmetric configurations, which necessitate a small time step and often require the inclusion of long memory. However, asymmetry values in the wings of the distribution enter with small coefficients and thus small deviations from converged results tend to be irrelevant. In each case, convergence with respect to the path integral parameters was verified. The calculations were performed with the SMatPI code,³⁶ with the SMatPI matrices computed using the kink sum algorithm, which takes advantage of the large spread of path weights (reflecting the number and type of kinks they contain) to bin the paths, leading to a dramatic acceleration of the path sum that allows calculations with very long memory.³²

In the case of a TLS, only the energy difference between the two diagonal elements is physically meaningful, thus the average could be calculated using a one-dimensional quadrature. However, larger systems require the evaluation of multidimensional integrals. Further, the set of system parameters may be available from molecular dynamics data on a non-uniform grid. For these reasons the test results are most suggestive if the averages are computed using a noisy algorithm. The SMatPI results for the state population $P_1 = \tilde{\rho}_{11,11}$ were averaged with respect to static disorder by sampling the distribution using 10000 Monte Carlo passes, i.e. a total of 10000 n realizations of the system Hamiltonian.

As a first example, consider a symmetric TLS with the Hamiltonian given in Eq. (8) with $\bar{H}_{11} = \bar{H}_{22} = 0$, where the two states are coupled to a common low-frequency bath with $\xi = 0.2$ and $\omega_c = 2\Omega$. It is assumed that only state φ_1 is populated at t=0 and that the bath is initially in thermal equilibrium at a low temperature specified by $\hbar\Omega\beta = 5$. Besides offering an excellent and simple model for studying the effects of a dissipative environment on tunneling dynamics, such a system characterizes the energy transfer dynamics in a molecular dimer, where each bath mode is the difference of the corresponding monomer normal mode coordinates. The electronic coupling is $500 \, \mathrm{cm}^{-1}$, with the chosen scaled parameters the peak of the spectral density is at $1000 \, \mathrm{cm}^{-1}$, and the temperature is $144 \, \mathrm{K}$. The total reorganization energy between the two states is $400 \, \mathrm{cm}^{-1}$.

Converged results for the RDM were obtained with $\Omega\Delta t=0.1$, $r_{\rm max}=L=15$. The populations were followed until the average value for $\sigma\leq 2$ reaches equilibrium, which involves 1000 time steps (although a shorter interval is shown). Figure 2 shows the evolution of P_1 for several different realizations of the system Hamiltonian, where the energy difference between the diagonal elements $H_{11}-H_{22}$ varies between $\pm 10\hbar\Omega$. In the absence of static disorder, the populations exhibit damped oscillatory dynamics. The symmetric TLS $(H_{11}-H_{22}=0)$ displays the most pronounced tunneling oscillations. As the energy

bias $H_{11}-H_{22}$ is increased on the positive side, P_1 decays to smaller values that reflect the equilibrium Boltzmann population. When $H_{11}-H_{22}$ is negative, φ_1 is the more stable of the two states, thus its population remains near unity. Figure 2 also shows the averaged state population for three values of static disorder, described by $\sigma=\hbar\Omega$, $\sigma=2\hbar\Omega$ and $\sigma=3\hbar\Omega$, and compares to the time evolution of this population for the symmetric TLS. Since σ describes the spread of each of the two site energies, the standard deviation of the energy gap $|H_{11}-H_{22}|$ is $\sigma\sqrt{2}$. Because the distribution of energy difference is symmetric, the long-time value of the average population must be equal to 0.5, and the Monte Carlo-averaged SMatPI results capture this value with impressive accuracy. It is seen that increasing disorder quenches the oscillatory component and prolongs the decay of P_1 to its equilibrium value. The averaged state population oscillates about positive values that shift higher with increasing σ . Furthermore, the oscillation peaks are shifted to shorter times, reflecting the larger value (blue shift) of the tunneling splitting with increasing asymmetry.

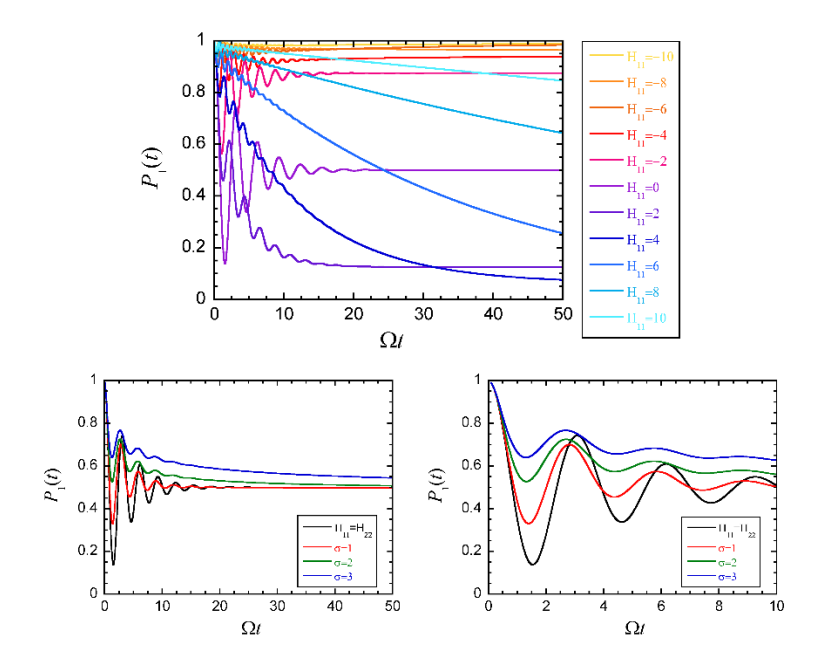


Fig. 2. Time evolution of P_1 and effects of static disorder for a symmetric TLS coupled to a harmonic bath with $\xi=0.2$, $\omega_{\rm c}=2\hbar\Omega$ at a temperature $\hbar\Omega\beta=5$. The top panel shows the populations for values of $H_{11}-H_{22}$ (in units of $\hbar\Omega$) that range between $\pm 10\hbar\Omega$. The bottom panels show averaged values for $\sigma=1,2$ and 3, along with the population in the absence of static disorder. The right panel shows the same results over short times.

The next example involves a model of excitation energy transfer in a molecular heterodimer. ^{7,41-42} The excited states of the two monomers have energies that differ by $\varepsilon = 520\,\mathrm{cm}^{-1}$ and are coupled by a parameter equal to $\hbar\Omega = 52\,\mathrm{cm}^{-1}$. The vibrational modes of each monomer constitute a harmonic bath modeled by an Ohmic spectral density with $\omega_c = 520\,\mathrm{cm}^{-1}$. The displacement between the ground and excited potential surfaces leads to a reorganization energy, chosen as $\lambda = 2080\,\mathrm{cm}^{-1}$, which corresponds to $\xi = 2$. The dimer is at a temperature $T = 300\,\mathrm{K}$, i.e. $\hbar\Omega\beta = 0.25$. Within the single excitation subspace, the energy transfer process is described by an asymmetric TLS Hamiltonian,

$$\hat{H}^{0} = \varepsilon |\varphi_{1}\rangle\langle\varphi_{1}| - \hbar\Omega(|\varphi_{1}\rangle\langle\varphi_{2}| + |\varphi_{2}\rangle\langle\varphi_{1}|)$$
(15)

where $\varepsilon = 10 \hbar \Omega$. The static disorder is assumed to have a standard deviation $\sigma = 260 \, \mathrm{cm}^{-1}$, i.e. $\sigma = 5 \hbar \Omega$. Because of the large reorganization energy, the system is in the activated regime for practically all arrangements of the donor/acceptor energies. The energy transfer process is assumed to start with excitation of the higher-energy monomer from the ground state by a Franck-Condon process.

The strong system-bath coupling, along with the large asymmetry of many TLS configurations that contribute for the chosen value of static disorder, necessitate a small time step and require the inclusion of long memory. Converged results were obtained with $\Omega\Delta t = 0.02$ and $r_{\rm max} = 35$. For the majority of sampled site energies, equilibrium was reached after approximately 70000 path integral time steps.

Figure 3 shows the population of the initially excited state as a function of time for site energies within $\pm 2\sigma$ ($|\Delta\varepsilon| = |\Delta\varepsilon_1 - \Delta\varepsilon_2| \le 10\hbar\Omega$) from the site energy gap of the bare system. For $\Delta\varepsilon = -10\hbar\Omega$ the TLS becomes symmetric and the long-time population becomes equal to 0.5. For even more negative values of $\Delta\varepsilon$ (not shown in the figure) the initially populated state has a lower energy, leading to equilibrium population values that exceed 0.5. Again, the broad range of energy gaps sampled by the function modeling static disorder leads to a wide spread of behaviors. When the energy gap is increased, the equilibrium population becomes smaller; further, the potential crossing point is lowered, leading to faster dynamics.⁴³ Conversely, a decrease of the energy gap leads to a larger donor equilibrium population but slower energy transfer.

The variety of time scales and long-time values implies that a significant number of system configurations must be sampled in order to obtain converged results. This is made clear in the right panel of Fig. 3, which shows the Gaussian distribution of energy gap values and the corresponding populations at a short time, an intermediate time, and at equilibrium. It is seen that these values are largest in the left wing of the distribution and continue to increase as the sampling function attains even smaller values. Converged results for the populations, averaged with respect to static disorder with 10000 Monte Carlo passes, i.e. 20000 Monte Carlo points, are shown in the left panel of Fig. 3.

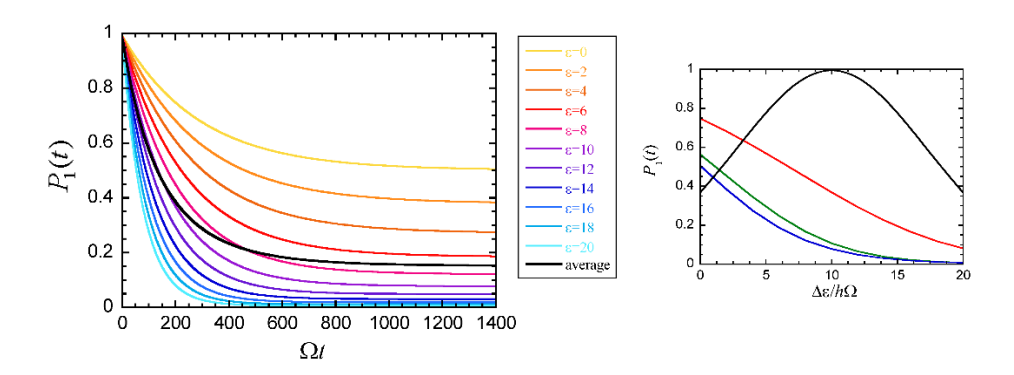


Fig. 3. Time evolution of P_1 and effect of static disorder in a model heterodimer with electronic coupling $\hbar\Omega=52\,\mathrm{cm}^{-1}$ at room temperature. The vibrational modes of the monomers are modeled by harmonic baths with $\omega_c=520~\mathrm{cm}^{-1}$ and excited-ground reorganization energies equal to $\lambda=2080\,\mathrm{cm}^{-1}$. The left panel shows (in units of $\hbar\Omega$) the populations for values of $\Delta\varepsilon$ that range between $\pm520\,\mathrm{cm}^{-1}$, as well as the averaged population for $\sigma=260\,\mathrm{cm}^{-1}$. The black line in the right panel shows the Gaussian distribution of the energy gap and the red, green and blue lines show the values of the populations at three time instants, $\Omega t=200$, 600 and 1400. It is seen that the distribution of population values is steeply skewed toward the left wing of the Gaussian distribution of energy gaps.

Last, consider the transfer of excitation energy in a trimeric aggregate within the normal mode approximation to the vibrations of each monomer. The electronic coupling is characterized by the parameter *J*, and the excited state of each monomer is displaced relative to the ground state, giving rise to exciton-vibration coupling. Within the single-excitation manifold, the energy transfer process is described by the Frenkel exciton Hamiltonian. In the absence of static disorder the monomers are assumed identical. Depending on the structure and relative orientation of the three monomers, the electronic coupling can be positive or negative. The initial excitation is placed on one of the monomers.

If the exciton-vibration coupling is neglected, the dynamics of excitation energy transfer does not depend on the sign of the electronic coupling. However, recent work⁴⁷⁻⁴⁸ found that the time evolution of electronic populations is much slower in the case of a trimer with J>0. This finding was explained⁴⁸ by the presence of a conical intersection between the ground and excited adiabatic states of this trimer, which leads to geometric phases that can significantly affect the dynamics.⁴⁹⁻⁵¹ The appearance of a conical intersection that involves the ground state is the consequence of electronic frustration,⁴⁷ the formation of a pair of degenerate states which are created because it is not possible to accommodate alternating signs in the wavefunction of a system with an odd number of units. The population of the initially excited state is shown in Figure 4 for a model trimer with vibrational baths characterized by the electronic coupling $J=\pm350\,\mathrm{cm}^{-1}$, spectral density peak at $\omega_c=1750\,\mathrm{cm}^{-1}$ and monomer reorganization energy $1050\,\mathrm{cm}^{-1}$ at a temperature $100\,\mathrm{K}$. The calculations were performed with $J/t/\hbar=0.125\,\mathrm{mod}\,r_{\mathrm{max}}=8,\,L=30\,\mathrm{cm}^{-1}$. Two distinct time scales are readily identified in the trimer with J>0. The early rapid decay is identical in the two trimers, but soon the population of the frustrated dimer switches to a much slower relaxation.

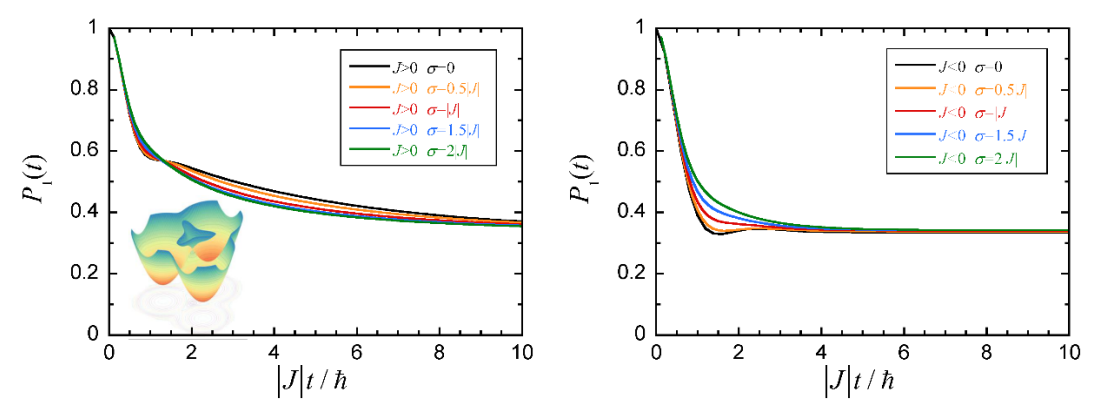


Fig. 4. Time evolution of P_1 and effect of static disorder on the energy transfer in a model trimer with electronic coupling $|J| = 350 \,\mathrm{cm}^{-1}$ at 100 K. The vibrational modes of the monomers are modeled by harmonic baths with $\omega_c = 1750 \,\mathrm{cm}^{-1}$ and excited-ground reorganization energies equal to $\lambda = 1050 \,\mathrm{cm}^{-1}$. Results are shown for three values of the disorder parameter, $\sigma = 175,350 \,\mathrm{and} \, 700 \,\mathrm{cm}^{-1}$. Top: $J = 350 \,\mathrm{cm}^{-1}$. Bottom: $J = -350 \,\mathrm{cm}^{-1}$. The inset shows the conical intersection in the case of J > 0.

Figure 4 also investigates the effects of static disorder in model trimers with opposite signs of J. With J < 0, the main effect of disorder is to shift the excited state population to higher values, in line with what was observed in Fig. 2 for a symmetric TLS. With J > 0 this trend is observed less prominently at short times, and is reversed after the onset of the slow decay. Static disorder breaks the symmetry of the trimer, lifting the degeneracy of electronic states. As the difference in electronic energies of the excited monomer increases, a gap develops between the adiabatic potential surfaces, gradually eliminating the slow kinetic component and leading to smoother energy transfer curves.

The acceleration attained through the EqC-PI formulation is most significant in the case of small systems with long memory (where the cost of each individual path sum tends to be high and the number of equivalence classes is relatively small) and increases linearly with the number of Hamiltonian realizations. For the numerical examples presented in this Letter, the gain in comparison to averaging the results of separate SMatPI calculations varied from approximately a factor of 65 (in the case of a trimer with $r_{\text{max}} = 8$) to 3500 (in the case of a TLS with $r_{\text{max}} = 35$).

In summary, it was shown that the effects of static disorder on the dynamics of a system coupled to one or multiple harmonic baths can be efficiently calculated via numerically exact real-time path integral methods, without computing the costly sum with respect to system paths for each realization of system Hamiltonians. This is achieved by grouping the discrete paths of the system into equivalence classes based on path connectivity, which are characterized by a common product of system propagators. By circumventing the need for performing a large number of expensive calculations to sample the desired distribution, the EqC-PI approach introduced in this Letter enables the inclusion of static disorder in accurate simulations that would otherwise be infeasible. While the numerical examples presented varied only the site energies, a variation of off-diagonal elements may be included without any modifications. The method is ideally suited to the efficient SMatPI propagation, in particular the kink sum algorithm, which may be used to treat very long memory in strongly coupled system-bath Hamiltonians.

The numerical examples presented reveal a wealth of nontrivial trends in the averaged results, such as upward or downward shifts of population curves, blue shifts and damping of oscillatory components, and significant changes of equilibration times and rates. Much further work is needed to characterize these intriguing effects, which are relevant to the dynamics of many experimentally studied systems. The algorithm presented in this Letter will facilitate such studies.

Last, the method is not restricted to system-bath Hamiltonians, and may be used in connection with any type of environment, provided the influence functional can be numerically evaluated (either by quantum mechanical⁵² or by semiclassical⁵³ methods).

Acknowledgment

This material is based upon work supported by the National Science Foundation under Award CHE-1955302.

References

- (1) Caldeira, A. O.; Leggett, A. J., Path integral approach to quantum Brownian motion. *Physica A* **1983**, *121*, 587-616.
- (2) Caldeira, A. O.; Leggett, A. J., Quantum tunnelling in a dissipative system. *Annals of Physics* **1983,** *149* (2), 374-456.
- (3) Weiss, U., *Quantum Dissipative Systems*. World Scientific: Singapore, 1993.
- (4) Ruf, B. A.; Miller, W. H., A new (Cartesian) reaction path model for dynamics in polyatomic systems, with application to H atom transfer in malonaldehyde. *J. Chem. Soc., Faraday Trans. 2* **1988**, 84, 1523-1534.
- (5) Miller, W. H.; Handy, N. C.; Adams, J. E., Reaction path Hamiltonian for polyatomic molecules. *J. Chem. Phys.* **1980**, *72*, 99-112.
- (6) Leggett, A. J.; Chakravarty, S.; Dorsey, A. T.; Fisher, M. P. A.; Garg, A.; Zwerger, W., Dynamics of the dissipative two-state system. *Rev. Mod. Phys.* **1987**, *59*, 1-85.
- (7) May, V.; Kühn, O., Charge and energy transfer dynamics in molecular systems. 3rd ed.; Wiley: 2011.
- (8) Chandler, D., *Introduction to Modern Statistical Mechanics*. Oxford University Press: New York, 1987.
- (9) Makri, N., The linear response approximation and its lowest order corrections: an influence functional approach. *J. Phys. Chem.* **1999**, *103*, 2823-2829.
- (10) Feynman, R. P., Space-time approach to non-relativistic quantum mechanics. *Rev. Mod. Phys.* **1948**, *20*, 367-387.
- (11) Feynman, R. P.; Hibbs, A. R., *Quantum Mechanics and Path Integrals*. McGraw-Hill: New York, 1965.
- (12) Feynman, R. P.; Vernon, F. L., The theory of a general quantum system interacting with a linear dissipative system. *Ann. Phys.* **1963**, *24*, 118-173.
- (13) Doll, J. D.; Freeman, D. L.; Beck, T. L., Equilibrium and dynamical Fourier path integral methods. *Adv. Chem. Phys.* **1990**, *78*, 61-127.
- (14) Makri, N., Feynman path integration in quantum dynamics. *Comp. Phys. Comm.* **1991**, *63*, 389-414.
- (15) Makri, N., Improved Feynman propagators on a grid and non-adiabatic corrections within the path integral framework. *Chem. Phys. Lett.* **1992**, *193*, 435-444.
- (16) Topaler, M.; Makri, N., System-specific discrete variable representations for path integral calculations with quasi-adiabatic propagators. *Chem. Phys. Lett.* **1993**, *210*, 448.
- (17) Light, J. C.; Hamilton, I. P.; Lill, J. V., Generalized discrete variable approximation in quantum mechanics. *J. Chem. Phys.* **1985**, *82*, 1400-1409.
- (18) Makri, N.; Makarov, D. E., Tensor multiplication for iterative quantum time evolution of reduced density matrices. I. Theory. *J. Chem. Phys.* **1995**, *102*, 4600-4610.
- (19) Makri, N.; Makarov, D. E., Tensor multiplication for iterative quantum time evolution of reduced density matrices. II. Numerical methodology. *J. Chem. Phys.* **1995**, *102*, 4611-4618.
- (20) Sim, E.; Makri, N., Tensor propagator with weight-selected paths for quantum dissipative dynamics with long-memory kernels. *Chem. Phys. Lett.* **1996**, *249*, 224-230.
- (21) Sim, E.; Makri, N., Filtered propagator functional for iterative dynamics of quantum dissipative systems. *Comp. Phys. Commun.* **1997**, *99*, 335-354.
- (22) Sim, E., Quantum dynamics for a system coupled to slow baths: on-the-fly filtered propagator method. *J. Chem. Phys.* **2001**, *115*, 4450-4456.
- (23) Lambert, R.; Makri, N., Memory path propagator matrix for long-time dissipative charge transport dynamics. *Mol. Phys.* **2012**, *110*, 1967-1975.
- (24) Richter, M.; Fingerhut, B. P., Coarse-grained representation of the quasiadiabatic propagator path integral for the treatment of non-Markovian long-time bath memory. *J. Chem. Phys.* **2017**, *146*, 214101.

- (25) Makri, N., Blip decomposition of the path integral: Exponential acceleration of real-time calculations for quantum dissipative systems. *J. Chem. Phys.* **2014**, *141*, 134117.
- (26) Strathearn, A.; Kirton, P.; Kilda, D.; Keeling, J.; Lovett, B. W., Efficient non-Markovian quantum dynamics using time-evolving matrix product operators. *Nature Communications* **2018**, *9*, 3322.
- (27) Lambert, R.; Makri, N., Quantum-classical path integral: Classical memory and weak quantum nonlocality. *J. Chem. Phys.* **2012**, *137*, 22A552.
- (28) Lambert, R.; Makri, N., Quantum-classical path integral: Numerical formulation. *J. Chem. Phys.* **2012,** *137*, 22A553.
- (29) Makri, N., Small matrix disentanglement of the path integral: overcoming the exponential tensor scaling with memory length. *J. Chem. Phys.* **2020**, *152*, 041104.
- (30) Makri, N., Small matrix path integral for system-bath dynamics. *J. Chem. Theory and Comput.* **2020**, *16*, 4038–4049.
- (31) Makri, N., Small matrix path integral with extended memory. *J. Chem. Theory and Comput.* **2021,** *17*, 1-6.
- (32) Makri, N., Kink sum for long-memory small matrix path integral dynamics. *J. Phys. Chem.* **2024**, *submitted*.
- (33) Makri, N., Topological aspects of system-bath Hamiltonians and a vector model for multisite systems coupled to local, correlated or common baths. *J. Chem. Phys.* **2023**, *158*, 144107.
- (34) Schulman, L. S., *Techniques and applications of path integration*. John Wiley and Sons: New York, 1981.
- (35) Makri, N., Numerical path integral techniques for long-time quantum dynamics of dissipative systems. *J. Math. Phys.* **1995,** *36*, 2430-2456.
- (36) Kundu, S.; Makri, N., PathSum: A C++ and Fortran suite of fully quantum mechanical real-time path integral methods for (multi-)system + bath dynamics. *The Journal of Chemical Physics* **2023**, *158* (22).
- (37) Piepho, S. B.; Krausz, E. R.; Schatz, P. N., Vibronic coupling model for calculation of mixed valence absorption profiles. *Journal of the American Chemical Society* **1978**, *100* (10), 2996-3005.
- (38) Tiwari, V.; Peters, W. K.; Jonas, D. M., Electronic energy transfer through non-adiabatic vibrational-electronic resonance. I. Theory for a dimer. *J. Chem. Phys.* **2017**, *147*, 154308.
- (39) Bose, A.; Makri, N., All-mode quantum-classical path integral simulation of bacteriochlorophyll dimer exciton-vibration dynamics *J. Phys. Chem.* **2020**, *124*, 5028-5038.
- (40) Kundu, S.; Makri, N., Intramolecular vibrations in excitation energy transfer: Insights from real-time path integral calculations. *Annual Review of Physical Chemistry* **2022**, *73* (1), 349-375.
- (41) Schröter, M.; Ivanov, S. D.; Schulze, J.; Polyutov, S. P.; Yan, Y.; Pullerits, T.; Kühn, O., Exciton–vibrational coupling in the dynamics and spectroscopy of Frenkel excitons in molecular aggregates. *Physics Reports* **2015**, *567*, 1-78.
- (42) Hestand, N. J.; Spano, F. C., Expanded Theory of H- and J-Molecular Aggregates: The Effects of Vibronic Coupling and Intermolecular Charge Transfer. *Chemical Reviews* **2018**, *118* (15), 7069-7163.
- (43) Marcus, R. A.; Sutin, N., Electron transfers in chemistry and biology. *Biochim. Biophys. Acta* **1985,** *811*, 265-322.
- (44) Frenkel, J., On the transformation of light into heat in solids. *Phys. Rev.* **1931,** *37*, 17.
- (45) Minami, T.; Tretiak, S.; Chernyak, V.; Mukamel, S., Frenkel-exciton Hamiltonian for dendrimeric nanostar. *Journal of Luminescence* **2000**, 87-89, 115-118.
- (46) Eder, T.; Stangl, T.; Gmelch, M.; Remmerssen, K.; Laux, D.; Höger, S.; Lupton, J. M.; Vogelsang, J., Switching between H- and J-type electronic coupling in single conjugated polymer aggregates. *Nature Communications* **2017**, *8* (1), 1641.
- (47) Dani, R.; Makri, N., Excitation energy transfer in bias-free dendrimers: Eigenstate structure, thermodynamics, and quantum evolution. *The Journal of Physical Chemistry C* **2022**, *126* (25), 10309-10319.
- (48) Makri, N., Electronic frustration, Berry's phase interference and slow dynamics in some tight-binding systems coupled to harmonic baths. *J. Phys. A* **2023**, *56*, 144001.

- (49) Althorpe, S. C., General explanation of geometric phase effects in reactive systems: Unwinding the nuclear wave function using simple topology. *The Journal of Chemical Physics* **2006**, *124* (8), 084105.
- (50) Althorpe, S. C.; Stecher, T.; Bouakline, F., Effect of the geometric phase on nuclear dynamics at a conical intersection: Extension of a recent topological approach from one to two coupled surfaces. *The Journal of Chemical Physics* **2008**, *129* (21), 214117.
- (51) Cina, J. A., Dynamics of an excitation-transfer trimer: Interference, coherence, Berry's phase development, and vibrational control of non-adiabaticity. *J. Chem. Phys.* **2023**, *158*, 124307.
- (52) Ilk, G.; Makri, N., Real time path integral methods for a system coupled to an anharmonic bath. *J. Chem. Phys.* **1994**, *101*, 6708.
- (53) Makri, N.; Thompson, K., Semiclassical influence functionals for quantum systems in anharmonic environments. *Chem. Phys. Lett.* **1998**, *291*, 101-109.